Supporting Information

3D Printed Water-stable Cd-doped $Cs_4MnBi_2Cl_{12}$/Polylactic Acid Perovskite/Polymer Composites for High-Flux X-ray Scintillation

Amr Elattar,*[a] Abdullah Al Noman,[a] Akil Dyson,[a] J.S. Raaj Vellore Winfred,[b] Burak Guzelturk,[c] Logan T. Kearney,[d] Adrienn Maria Szucs,[e] and Tarik Dickens*[a]

Supplemental figures

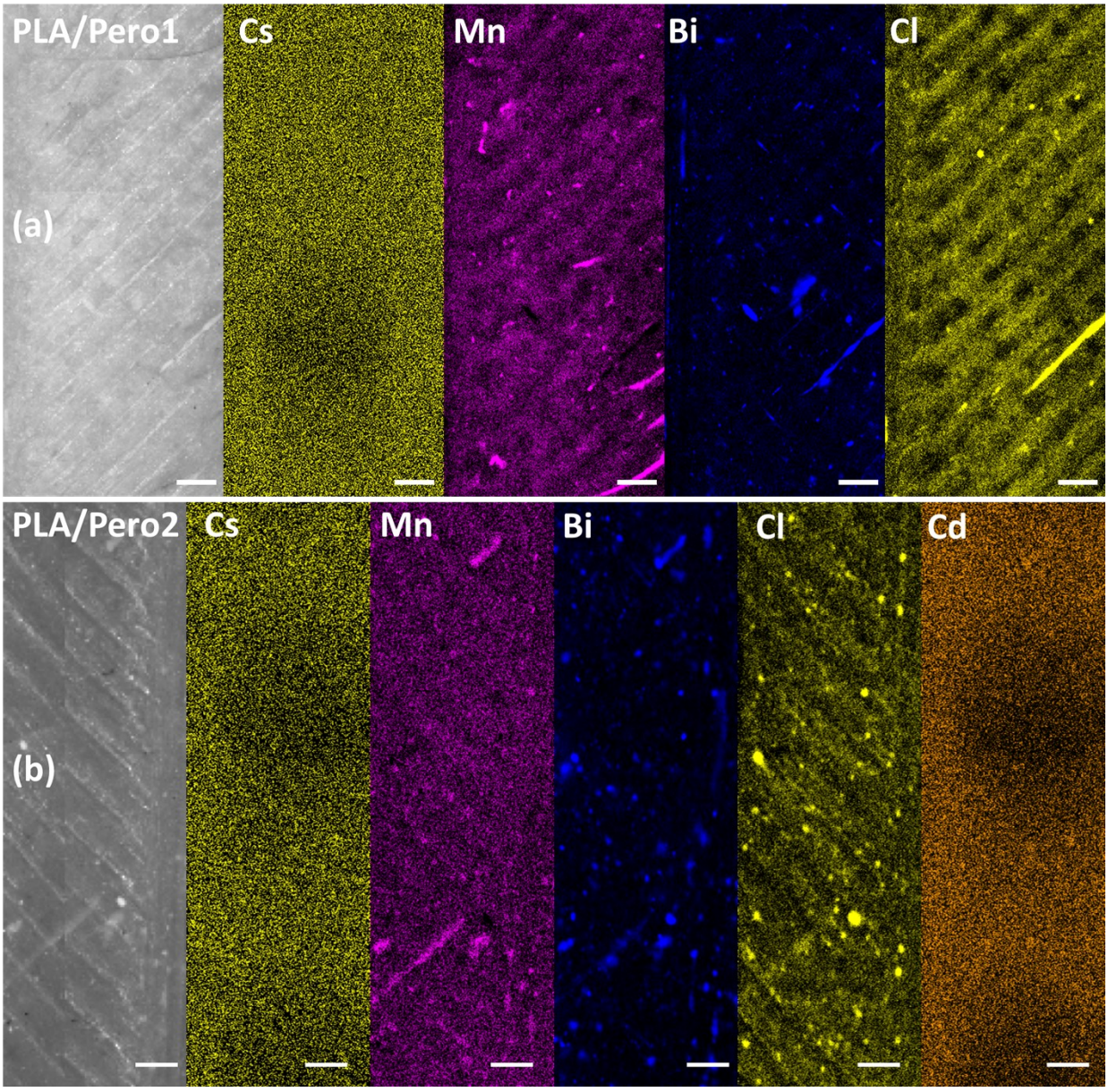

Fig. S1 X-ray fluorescence (XRF) mapping of PLA/Pero1 and PLA/Pero2 films (Scale bar = 1000 μm).

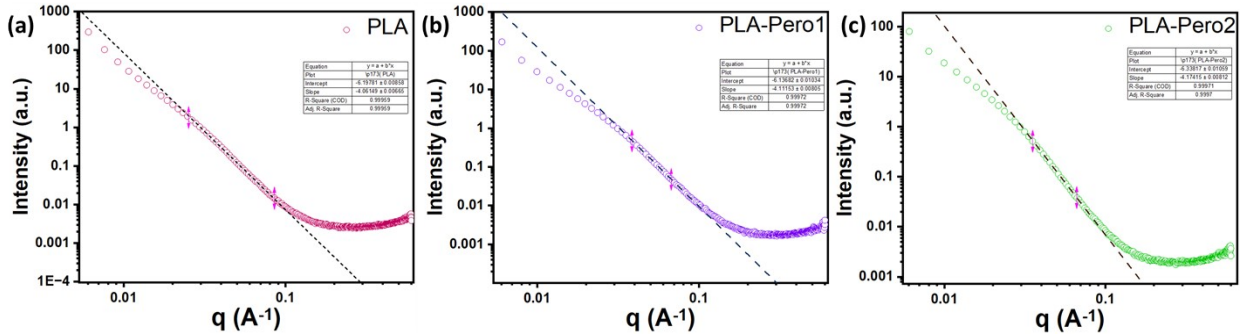

Fig. S2 SAXS measurement of PLA (a), PLA-Pero1 (b), and PLA-Pero2 (c) composites.

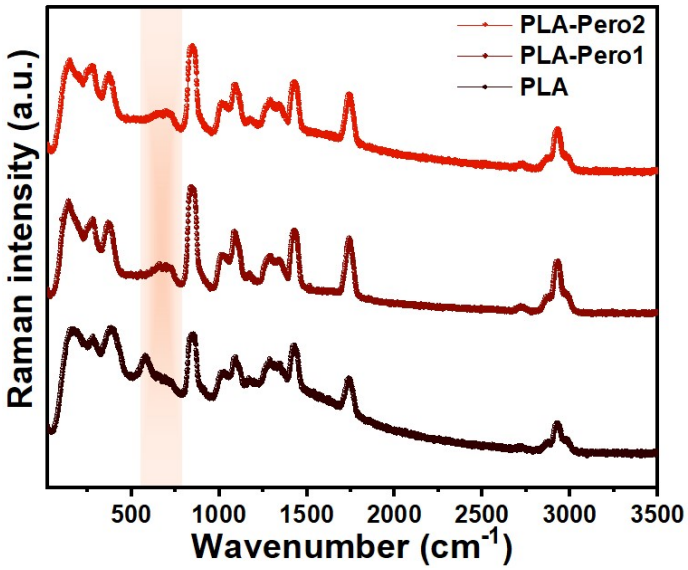

Fig. S3 Raman spectra of PLA-Pero composites.

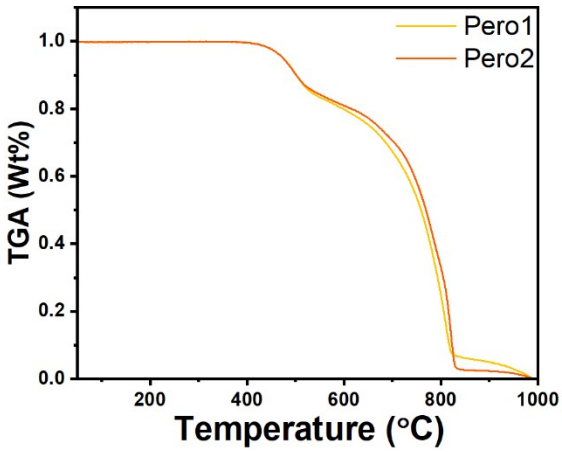

Fig. S4 Thermogravimetric analysis (TGA) of Pero1 and Pero2 powders.

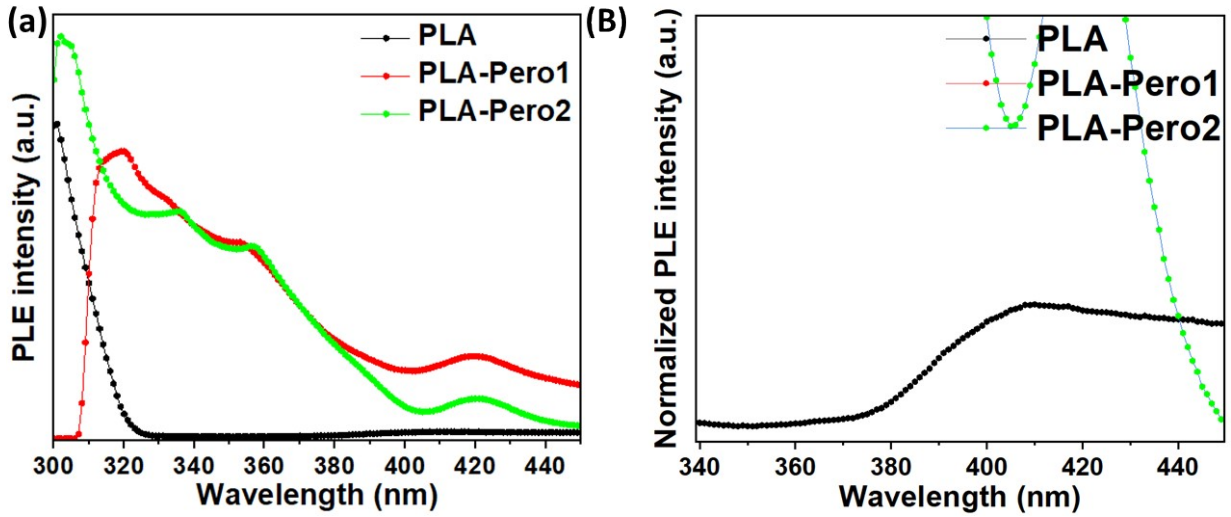

Fig. S5 Photoluminescence excitation PLE spectra of PLA-Pero composites (a) and zoom-in to show the second excitation peak of the PLA sample (b).

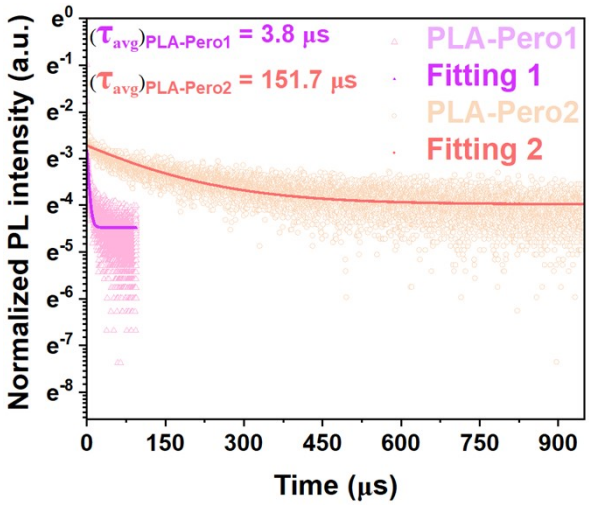

Fig. S6 Time-resolved PL spectra of PLA-Pero composites.

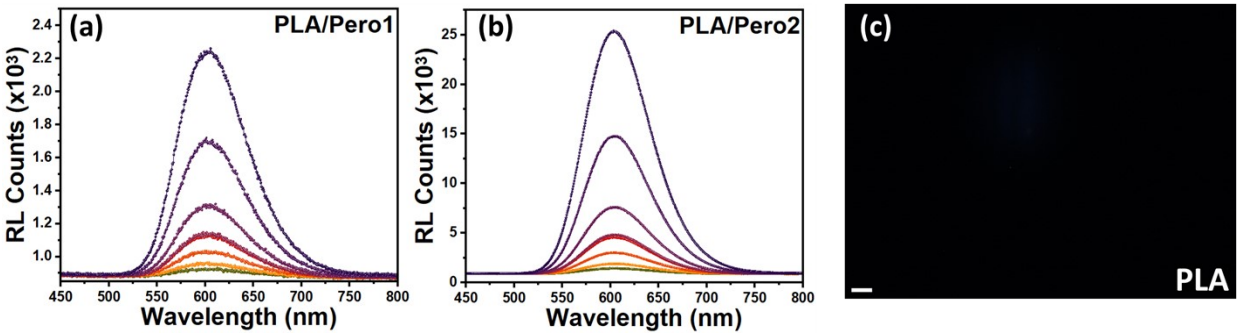

Fig. S7 (a, b) RL spectra at different absorbed X-ray flux in PLA/Pero1 and PLA/Pero2 samples, respectively. (c) X-ray image of 5 LP mm-1 target with the PLA film.

Supplemental tables

Table S1. Atomic ratios of perovskite elements obtained through XRF mapping

Atomic ratio	Cs	Mn	Bi	Cd	Cl
PLA-Pero1	0.97	0.32	0.77	w/o	1.27
PLA-Pero2	18.35	2.27	13.64	1.07	16.28

Table S2. Raman Bands and their corresponding modes of perovskite powders.

Raman Band	Raman Wavelength (cm^{-1})	Vibrational mode
Y1	125.3	The scissoring modes of $[BiCl_6]^{3-}$& $[MnCl_6]^{4-}$
Y2	153.2	
Y3	248.1	The vibrational asymmetric stretching mode (Eg) of $[BiCl_6]^{3-}$& $[MnCl_6]^{4-}$
Y4	273.8	The stretching mode (A1g) of $[CdCl_6]^{4-}$
Y5	295.4	The vibrational symmetric stretching mode (A1g) of $[BiCl_6]^{3-}$& $[MnCl_6]^{4-}$

Table S3. Comparison of excitation spectral features among PLA-perovskite composites

Peaks	PLA	PLA-Pero1	PLA-Pero2
Peak1	300 nm	319 nm	301 nm
Peak2	-	332 nm	335 nm
Peak3	-	353 nm	357 nm
Peak4	410 nm	419 nm	420 nm

Table S4. Time-resolved PL-spectra parameters

B_1	τ_1	B_2	τ_2	τ_{AVG}
-0.02985	3.8006	0.08688	3.8002	3.799991
-0.02412	151.7252	0.07142	151.709	151.7008

Table S5. Comparison of the X-ray scintillation parameters of our samples with those of other representative scintillators.

Compound	Dose rate	LY (photons MeV^{-1})	Spatial resolution (lp/mm @MTF=0.2)	Reference
$Cs_4MnBi_2Cl_{12}$ single crystal	Low	-	-	[1]
$(TEA)_2MnI_4$	Low	26288	25	[2]
$(BPTP)_2MnBr_4$/Epoxy resin	Low	136000	10.1	[3]
Glassy $(HTPP)_2MnBr_4$	Low	23300	10	[4]
$(C_{19}H_{18}P)_2MnBr_4$/PAN	Low	44000	12.6	[5]
$(C_8H_{20}N)_2MnBr_4$/Sucrose octaacetate	Low	24400	5	[6]
Glassy $(HTP)_2MnBr_4$	Low	38000	17.28	[7]
$(ETP)_2MnBr_4$	Low	35000	13.4	[8]
$(MTP)_2MnBr_4$	Low	67000	6.2	[9]
Br-$CsCdCl_3$/PDMS	Low	43000	14.8	[10]
$Cs_4Mn_{0.32}Cd_{0.68}Bi_2Cl_{12}$ /PLA	High	-	5	This work

References

1 Dun C, Ma J, Zhang M, Ji H, Su M, Xing X *et al.* High-temperature stable and sensitive X-ray detector based on two-dimensional lead-free perovskite Cs4MnBi2Cl12 single crystal. *Nano Res* 2025; 18. doi:10.26599/NR.2025.94907574.

2 Zhang Z-Z, Wei J-H, Luo J-B, Wang X-D, He Z-L, Kuang D-B. Large-Area Laminar TEA2MnI4 Single-Crystal Scintillator for X-ray Imaging with Impressive High Resolution. *ACS Appl Mater Interfaces* 2022; 14: 47913–47921.

3 Zhang R, Xie H, Liu W, Zhan K, Liu H, Tang Z *et al.* High-Efficiency Narrow-Band Green-Emitting Manganese(II) Halide for Multifunctional Applications. *ACS Appl Mater Interfaces* 2023; 15: 47238–47249.

4 Luo J-B, Wei J-H, Zhang Z-Z, He Z-L, Kuang D-B. A Melt-Quenched Luminescent Glass of an Organic–Inorganic Manganese Halide as a Large-Area Scintillator for Radiation Detection. *Angewandte Chemie International Edition* 2023; 62: e202216504.

5 Zheng G, Bao Z, Liu L, Xu L, Cheong KY, Zheng Z *et al.* Lead-free X-ray imaging scintillators based on zero-dimensional manganese hybrid metal halide. *Chemical Engineering Journal* 2025; 525: 170130.

6 Jiang T, Ma W, Zhang H, Tian Y, Lin G, Xiao W *et al.* Highly Efficient and Tunable Emission of Lead-Free Manganese Halides toward White Light-Emitting Diode and X-Ray Scintillation Applications. *Adv Funct Mater* 2021; 31: 2009973.

7 Xu Y, Li Z, Peng G, Qiu F, Li Z, Lei Y *et al.* Organic Cation Design of Manganese Halide Hybrids Glass toward Low-Temperature Integrated Efficient, Scaling, and Reproducible X-Ray Detector. *Adv Opt Mater* 2023; 11: 2300216.

8 Li B, Xu Y, Zhang X, Han K, Jin J, Xia Z. Zero-Dimensional Luminescent Metal Halide Hybrids Enabling Bulk Transparent Medium as Large-Area X-Ray Scintillators. *Adv Opt Mater* 2022; 10: 2102793.

9 Zhang W, Sui P, Zheng W, Li L, Wang S, Huang P *et al.* Pseudo-2D Layered Organic-Inorganic Manganese Bromide with a Near-Unity Photoluminescence Quantum Yield for White Light-Emitting Diode and X-Ray Scintillator. *Angewandte Chemie International Edition* 2023; 62: e202309230.

10 Peng H, Kong L, Li X, Wei Q, Zhao X, Chen B *et al.* Portable and Visualized X-ray Dose Rate Detection and Imaging Utilizing Br-Doped CsCdCl3 Crystals. *ACS Appl Mater Interfaces* 2025; 17: 59625–59636.